

Ti3C2Tx MXenes: From Recovery of Pb from Perovskite Solar Cells to Supercapacitor Usage

Downloaded from: https://research.chalmers.se, 2025-11-30 21:16 UTC

Citation for the original published paper (version of record):

Andrade, M., Mezzetti, A., Fumagalli, F. et al (2025). Ti3C2Tx MXenes: From Recovery of Pb from Perovskite Solar Cells to Supercapacitor Usage. Journal of the Electrochemical Society, 172(11). http://dx.doi.org/10.1149/1945-7111/ae1ad5

N.B. When citing this work, cite the original published paper.

research.chalmers.se offers the possibility of retrieving research publications produced at Chalmers University of Technology. It covers all kind of research output: articles, dissertations, conference papers, reports etc. since 2004. research.chalmers.se is administrated and maintained by Chalmers Library



OPEN ACCESS

Ti₃C₂T_x MXenes: From Recovery of Pb from Perovskite Solar Cells to Supercapacitor Usage

To cite this article: Marcelo A. Andrade et al 2025 J. Electrochem. Soc. 172 110519

View the article online for updates and enhancements.

You may also like

- Mesoscale Design Principles for Graphite <u>Electrodes Enabled by 3D Heterogeneous</u> <u>Modeling of Ellipsoidal Particles</u> Junyi Qi, Anhao Zuo, Ruqing Fang et al.
- Physico-Chemical and Electrochemical Analysis of Hard-Carbon From Licorice Root Bio-Waste as Anode for Sodium Ion Batteries

Asia Patriarchi, Leonardo Sbrascini, Jonathan Caroni et al

- Effect of Ionomer-to-Carbon Ratio on PEMFC Carbon Corrosion: An Electrochemical Study Sebastian Raab, Ayon Karmakar, Po-Ya Abel Chuang et al.

Your Lab in a Box!

The PAT-Tester-i-16 Multi-Channel Potentiostat for Battery Material Testing!

- ✓ All-in-One Solution with Integrated Temperature Chamber (+10 to +80 °C)! No additional devices are required to measure at a stable ambient temperature.
- ✓ Fully Featured Multi-Channel Potentiostat / Galvanostat / EIS!

 Up to 16 independent battery test channels, no multiplexing.
- ✓ Ideally Suited for High-Precision Coulometry! Measure with excellent accuracy and signal-to-noise ratio.
- ✓ Small Footprint, Easy to Setup and Operate! Cableless connection of 3-electrode battery test cells. Powerful EL-Software included.



electrochemical test equipm

Learn more on our product website:



Download the data sheet (PDF):



Or contact us directly:

- +49 40 79012-734
- www.el-cell.com





Ti₃C₂T_x MXenes: From Recovery of Pb from Perovskite Solar Cells to Supercapacitor Usage

Marcelo A. Andrade, ^{1,2} Alessandro Mezzetti, ³ Francesco Fumagalli, ³ Giacomo Ceccone, ³ Olivier Crosnier, ^{1,2} Patrik Johansson, ^{4,5,6} and Thierry Brousse ^{1,2,*,2}

Sustainable disposal and valorization of recovered lead from end-of-life perovskite solar cells (PSCs) remain critical challenges from environmental and electrochemical perspectives. Here, we demonstrate a dual-function process wherein $T_{i3}C_2T_x$ MXenes adsorbents are first employed to recover lead from green acetone-based PSC recycling waste and subsequently repurposed as high-performant supercapacitor electrode active materials. Remarkably, $T_{i3}C_2T_x$ achieves >99.9% Pb²⁺ ion removal from 100 ppm Pb/ acetone solutions, with an adsorption capacity reaching up to 555 mg·g⁻¹. After adsorption, the Pb-loaded MXene ($T_{i3}C_2T_x/Pb_{ads}$) retains its structural integrity and exhibits significantly enhanced electrochemical performance. Electrochemical cycling in a sodium acetate aqueous electrolyte reveals a doubled specific capacity of the MXenes, from ca. 30 C·g⁻¹ to ca. $60C\cdot g^{-1}$, by introducing reversible Pb²⁺/Pb⁰ redox activity while maintaining the initial MXene pseudocapacitive behavior. Overall, this conceptual study demonstrates a closed circular materials loop by recovering a green solvent from the PSC recycling, while transforming a hazardous waste stream into a value-added energy storage material.

© 2025 The Author(s). Published on behalf of The Electrochemical Society by IOP Publishing Limited. This is an open access article distributed under the terms of the Creative Commons Attribution 4.0 License (CC BY, https://creativecommons.org/licenses/by/4.0/), which permits unrestricted reuse of the work in any medium, provided the original work is properly cited. [DOI: 10.1149/1945-7111/ae1ad5]

Manuscript submitted August 27, 2025; revised manuscript received October 24, 2025. Published November 12, 2025.

Supplementary material for this article is available online

First introduced in 2009 and rapidly growing ever since, perovskite solar cells (PSCs) are a third-generation photovoltaic technology that utilizes thin films of hybrid organic-inorganic materials to provide efficient devices with reduced fabrication costs. In the last few years PSCs have reached the same conversion efficiencies of silicon-based solar cells-the current industrial standard-and the technology is moving towards full-scale production and commercialization.² Among the different compositions of PSCs, those based on Pb are the most likely studied such as CH₃NH₃PbI₃, CH₃NH₃PbI_{3-x}Cl_x, CH₃NH₃PbBr₃, $CH_3NH_3Pb(I_{1-X}Br_x)_3$, $HC(NH_2)_2PbI_3$, $HC(NH_2)_2Pb(I_{1-X}Br_x)_3$. $^{3-5}$ Fundamental calculations 6,7 as well as more applied studies $^{8-10}$ have been dedicated to these materials. Despite the clear advantages of high efficiencies and contained costs, the PSC technology still has to address two crucial issues that otherwise could hinder its effective scalability and diffusion: stability and recycling. ¹¹ While stability is a multi-factor issue that includes complex phenomena such as material photodegradation, environmental influence, and thermal stresses, recycling is an issue mainly related to the presence of lead in the high-performant PSCs. 12

Plenty of research has been devoted to PSC recycling to develop processes and methods that can effectively segregate and sequester lead from end-of-life devices for safe disposal, whilst also recovering functional and reusable components. The most common method is chemical dissolution via a solvent bath, usually performed using dimethylformamide (DMF)—the main solvent used in PSC manufacturing—due to its fast kinetics and high lead solubility. ¹³ The use of DMF is, however, complicated due to its high toxicity and environmental impact. At the same time, more viable alternatives have been found by using greener and safer solvents belonging to the polar aprotic family. ¹⁴

Regardless of the method chosen, the main output is contaminated solvents that contain all the compounds removed from the PSCs, and foremost, high concentrations of lead. According to

these contaminated solvents is safe disposal, since recovery of any dissolved compounds, including lead, for reuse in PSC manufacturing is not worth the effort due to the complexity and overall cost. ^{15,16} However, mindful of the old adage "one man's trash is another man's treasure," we have found a way to generate value from these contaminated solvents: by adsorbing the dissolved lead using specific MXenes (see below), we can regenerate the solvent used in the recycling process, and as a further benefit also improve the electrochemical performance of the this way-enriched MXenes, for subsequent use as supercapacitor electrode active materials. ^{17,18}

MXenes are a class of two-dimensional transition metal carbides

different techno-economic analyses, the only practical use for

MXenes are a class of two-dimensional transition metal carbides or nitrides, known for their high surface area, metallic conductivity, hydrophilicity, and tunable surface chemistry, which make them attractive for a broad range of applications, including energy storage^{19–23} and water purification.²⁴ Due to their negatively charged surfaces and abundant functional groups, MXenes can effectively bind heavy metal ions, such as Pb²⁺, Hg²⁺, and Cr⁶⁺, from aqueous and organic media.^{25,26} The MXene-metal ion interactions can occur through several mechanisms, including surface complexation, electrostatic attraction, ion exchange, and redox reactions, depending on the functional groups present on the MXene surface and the metal ion at hand. In particular, carboxyl, hydroxyl, and oxygenated groups on MXenes can act as chelating agents, while the interlayer spacing between MXene sheets can host intercalated species.^{27–30}

In a recent work, Shah et al. synthesized and employed carboxylic-terminated $Ti_3C_2T_x$ MXene nanosheets as efficient adsorbents for the removal of toxic Cr^{6+} and Pb^{2+} ions from aqueous media. Synthesized via citric acid-assisted etching, the MXene exhibited exceptional adsorption capacities of 1090 mg·g $^{-1}$ for Cr (VI) and $1135\ mg\cdot g^{-1}$ for Pb(II), with equilibrium times of only 7 and 4 min, respectively. The adsorption process was best described by the Freundlich isotherm, indicating multilayer adsorption on heterogeneous surfaces driven by electrostatic interactions and ion exchange via –COOH and –OH functional groups.

¹Nantes Université, CNRS, Institut des Matériaux de Nantes Jean Rouxel, IMN, Nantes, France

²Réseau sur le Stockage Electrochimique de l'Energie (RS2E), FR CNRS 3459, Hub de l'Energie, 80039 Amiens, France

³European Commission, Joint Research Centre (JRC), Ispra, Italy

⁴Alistore-ERI European Research Institute, FR CNRS 3104, Hub de l'Energie, 80039 Amiens, France

⁵Department of Physics, Chalmers University of Technology, SE-412 96 Gothenburg, Sweden

⁶Department of Chemistry - Ångström, Uppsala University, SE-751 20 Uppsala, Sweden

^{*}Electrochemical Society Fellow.

^zE-mail: thierry.brousse@univ-nantes.fr

This work follows the proof-of-concept study on recycling spent heavy metal-containing wastewater adsorbents as electrodes for energy storage,³² and the positive results reported in literature for PSC recycling using greener and safer polar aprotic solvents such as DMSO and acetone. ^{33,34} Given its cheaper cost, easier availability, and safer handling, acetone has been chosen as the polar aprotic solvent employed in this study. Herein, MXenes are used as adsorbents from a model contaminated acetone used to dissolve lead iodide (PbI₂), the same lead compound as used in the majority of high-performance PSCs. The solvent is recovered with a minimum concentration of dissolved lead remaining, reducing the costs and complexity of handling and disposing of it,³⁵ and the Pbloaded MXenes are recycled into electrochemical energy storage electrodes, with improved capacities thanks to the adsorbed lead. Namely, supercapacitor electrodes with enhanced performance have been prepared using recycled MXene absorbents. Interestingly, the coupling of PSCs and supercapacitors have already been proposed in the literature, ^{36–41} but this study offers for the first time the opportunity to design a supercapacitor with recycled PSCs that could be in turn coupled with a new PSCs.

Results and Discussion

Lead adsorption.—To perform the lead adsorption experiments in a consistent and effective way, large volumes of contaminated solvent were required, with precise control over their lead concentration. To this end, model solutions referred to as "Pb/acetone solutions" were prepared by dissolving lead iodide and sodium iodide into acetone. The amount of lead iodide was calculated to obtain the desired level of lead concentration, whereas sodium iodide was added to enable the complete dissolution of the lead salt. Strong donor solvents such as DMF can dissolve lead iodide at high concentrations due to the formation of donor-acceptor complexes, while weak donor solvents such as acetone need an addition of iodine ions (provided by sodium iodide) to promote the formation of iodoplumbate complexes solvated via strong ion-dipole interaction with the solvent. 42

The Pb/acetone solutions thus prepared might be considered an oversimplification when compared to the actual contaminated solutions that are obtained from recycling, since they lack all the additional compounds that are dissolved from a full PSC device, and thus all the possible interactions between these materials. However, this compromise allows for precise control of the concentration of the dissolved lead, and to prepare significant volumes of solution without the need to actually recycle and dissolve an exorbitant—and thus impracticable—number of PSC devices. For the sake of this explorative study, this simplified formulation was deemed suitable and satisfactory.

For the lead adsorption experiments, the Pb/acetone solutions were first tested with different known adsorbents, selected based on their known affinity to lead cations in aqueous media. ^{31,43,44} In order to assess their adsorption capacity in the acetone medium, different vials of 100 ppm Pb/acetone solution were treated with reduced graphene oxide (rGO), and with decreasing doses of titanium carbide MXenes, sourced from two different synthetic routes that use LiF and NH₄HF₂ as the etching agents, respectively named Ti₃C₂T_x-LiF and Ti₃C₂T_x-NH₄HF₂. Ti₃C₂T_x-LiF was the preferred choice for further study and processing due to its demonstrated high affinity to lead in solution and a much simpler synthesis procedure, which dismisses the exfoliation step, leading to much higher yields. ^{45,46} The mass percentage of lead captured is shown as a function of adsorbent dose (*d*, mg·L⁻¹) in Fig. 1.

Compared at the highest dose of $1 \text{ g} \cdot \text{L}^{-1}$ of adsorbent, rGO was able to remove about 34% of the lead, while $\text{Ti}_3\text{C}_2\text{T}_x$ -LiF MXene adsorbed >99.9%. The adsorption capacity of $\text{Ti}_3\text{C}_2\text{T}_x$ -LiF remained steadily >95% as the dose was lowered down to 250 mg·L⁻¹, before decreasing to ca. 36% for the lowest dose of 100 mg of MXene adsorbent powder per liter of Pb/acetone solution. At the same low dose, $\text{Ti}_3\text{C}_2\text{T}_x$ -NH₄HF₂ performed similarly to the one synthesized

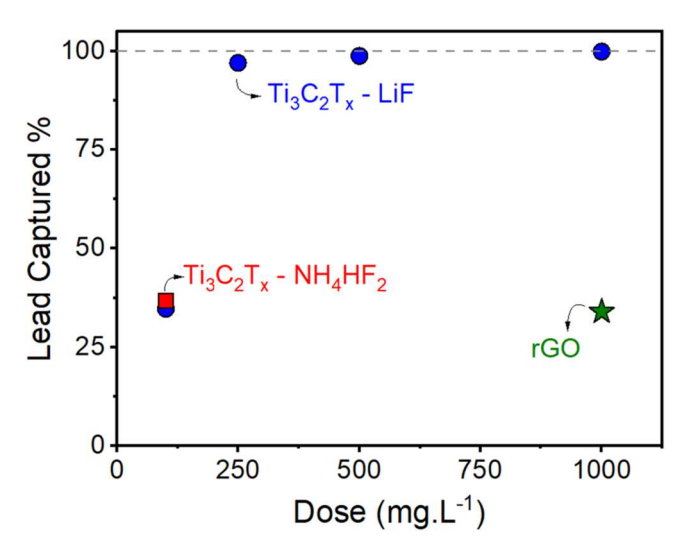


Figure 1. Percentage of Pb removed at equilibrium from 100 ppm Pb/ acetone solutions using reduced graphene oxide (rGO), Ti₃C₂T_x-NH₄HF₂, and Ti₃C₂T_x-LiF with different doses.

using LiF, reaching a lead removal capacity of ca. 37%. The slightly higher adsorption performance of $Ti_3C_2T_x$ -NH₄HF₂, however, does not justify its choice given the much simpler and more straightforward synthesis of $Ti_3C_2T_x$ -LiF.

Following the initial adsorption studies, $\text{Ti}_3\text{C}_2\text{T}_x$ -LiF adsorption performance was compared to $\text{Ti}_3\text{C}_2\text{T}_x$ -NH₄HF₂ by varying the initial Pb concentration (C_0 , $\text{mg}\cdot\text{L}^{-1}$) while keeping the same adsorbent dose. The adsorption capacity at equilibrium ($q_e/\text{mg}\cdot\text{g}^{-1}$) is shown as a function of the remaining lead concentration at equilibrium (C_e , $\text{mg}\cdot\text{L}^{-1}$), presented as adsorption isotherms in Fig. 2.

There is a clear trend on both isotherms, as the increase in initial Pb concentration leads to an increased adsorption capacity. Both MXenes reached impressive adsorption capacities of lead, up to 490 and $555~{\rm mg\cdot g^{-1}}$ for ${\rm Ti_3C_2T_x\text{--}LiF}$ and ${\rm Ti_3C_2T_x\text{--}NH_4HF_2}$, respectively. Langmuir and the Freundlich equations below (Eqs. 1 and 2, respectively) do not directly fit the experimental data, but describe well the isotherms' trends.

$$q_e = \frac{q_{\text{max}} K_L C_e}{1 + K_L C_e} \tag{1}$$

$$q_e = K_F C_e^{\frac{1}{n}}$$
 [2]

The Freundlich model fit returned a $R^2=0.81$ for $Ti_3C_2T_x$ -LiF and >0.84 for $Ti_3C_2T_x$ -NH₄HF₂. The maximum adsorption capacity $(q_{max}, mg \cdot g^{-1})$ was calculated for $Ti_3C_2T_x$ -NH₄HF₂ using Eq. 1, with a value of $q_{max}=672~mg \cdot g^{-1}$, which is close to the maximum obtained q_e , indicating that the saturation of the adsorbent was approached. Furthermore, the adsorption trend described by both models shows that Pb can be either physisorbed on the carbide surface or chemisorbed by the high presence of carboxylic-acid functional groups.³¹

Materials characterization.—After the lead adsorption studies detailed above, $Ti_3C_2T_x$ -LiF was chosen for further characterization. In order to characterize the pristine adsorbent (here named simply as $Ti_3C_2T_x$) and compare it with the one loaded with lead $(Ti_3C_2T_x/Pb_{ads})$, the materials were subjected to Raman spectroscopy and X-ray diffraction (XRD) analyses (Fig. 3).

The Raman spectrum obtained for $Ti_3C_2T_x$ is characteristic of that for these MXenes. There is a small resonance peak at $123~{\rm cm}^{-1}$, followed by the sharp A_{1g} peak at around $206~{\rm cm}^{-1}$, confirming the effective etching of MAX phases. The wide bands

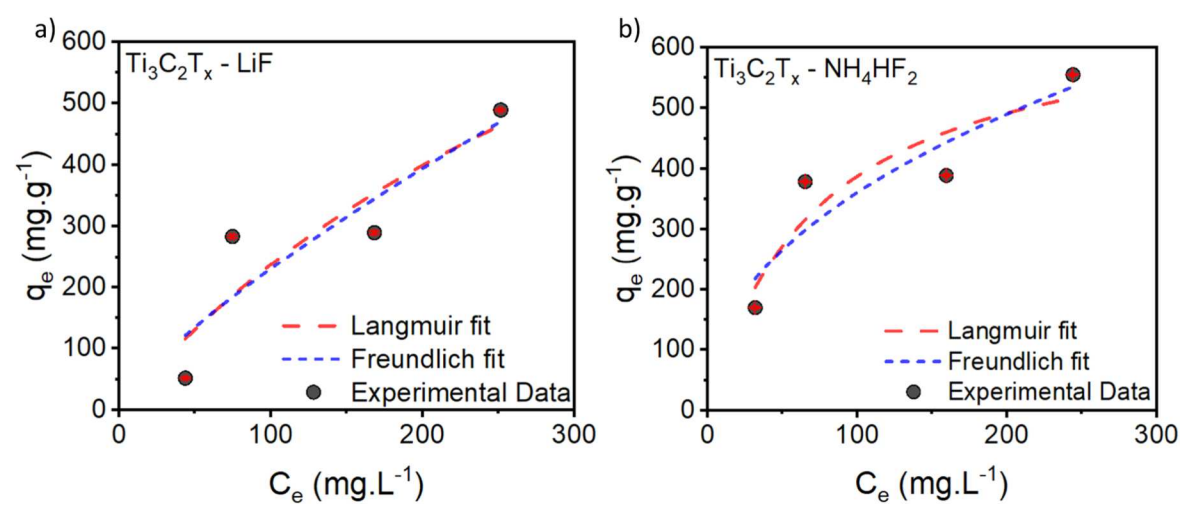


Figure 2. Adsorption isotherms for lead in Pb/Acetone solutions with $C_0 = 50$, 100, 200, and 300 ppm, $d = 100 \text{ mg} \cdot L^{-1}$ using a) $Ti_3C_2T_x$ —LiF and b) $Ti_3C_2T_x$ -NH₄HF₂ as adsorbents at 25 °C. The smaller graphs on the right side show the linearized versions of Langmuir (up) and Freundlich (bottom) plots.

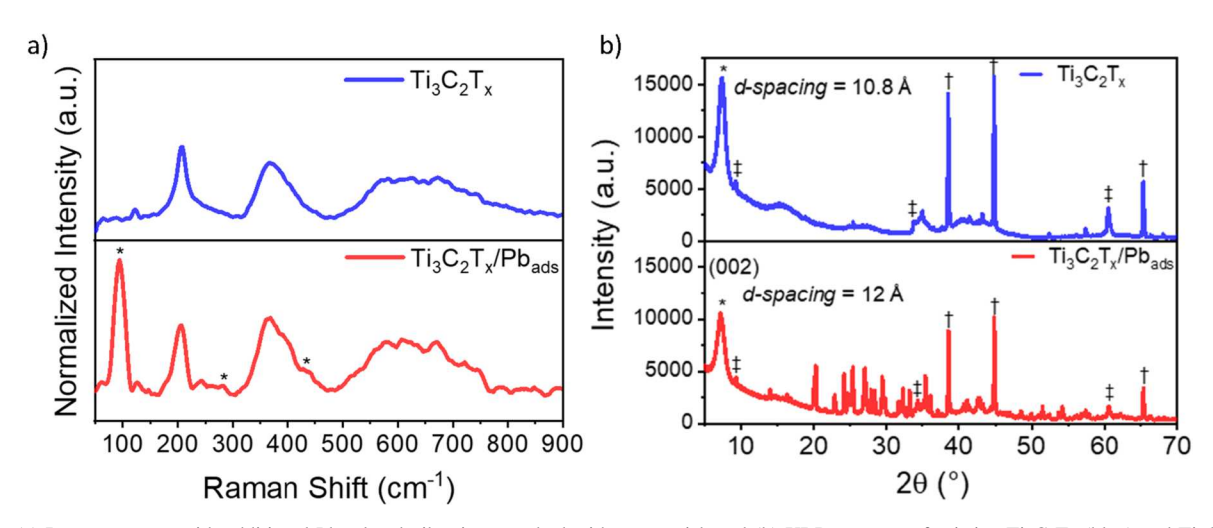


Figure 3. (a) Raman spectra with additional Pb-related vibrations marked with an asterisk and (b) XRD patterns of pristine $Ti_3C_2T_x$ (blue) and $Ti_3C_2T_x/Pb_{ads}$ (red) with (*) - MXene interlayer spacing, (†) - LiF griceite, and (‡) - MAX phase.

starting from $365\,\mathrm{cm}^{-1}$ relate to the in-plane (Eg) vibrations of the functional groups at the surface of the flakes, while the region starting from $576\,\mathrm{cm}^{-1}$ relates to both Eg and Alg from carbon vibrations. Slight changes between the pristine and Pb-loaded materials can be noted on the spectra, more specifically, additional vibrations at $95\,\mathrm{cm}^{-1}$, $284\,\mathrm{cm}^{-1}$, and $434\,\mathrm{cm}^{-1}$ marked with an asterisk. The last two are probably a result of the interaction between adsorbed lead and surface terminations, as they appear particularly in the functional group sensitivity region. The sharp peak at $95\,\mathrm{cm}^{-1}$ was associated with the small presence of lead iodide in the recovered powder. 50

Both synthesis processes using NH₄HF₂ and LiF as etchants lead to negatively charged surface compounds due to the presence of oxygenated functional groups. Therefore, the positively charged lead ions dispersed in the acetone solution are attracted to the MXene active surface sites, binding with them through either chelation and ionic exchange due to electrostatic attractions or by reacting with the functional groups on the surface. The presence of hydroxyl functional groups enhances the surface properties in terms of reactivity and hydrophilicity, possibly improving the ion exchange mechanism of the metal ions and the sorption mechanism.^{51,52}

Both XRD patterns present the characteristic (002) broad peak, related to the *d-spacing* of the MXene, which represents the

combined thickness of a single MXene layer, surface terminations, and intercalated species, which is marked with an asterisk. ^{30,53} By subtracting the known thickness of an individual MXene layer (9.4 Å) from the *d-spacing*, the interlayer spacing is calculated. ⁵⁴ The calculated interlayer spacing for the materials increases by 0.6 Å upon lead adsorption, which is too little to indicate any lead intercalation between the multi-layered material. MXenes *d-spacing*, however, can be shifted depending on the hydration level of the powders, other intercalating salts, or even drying conditions, representing a challenge to confirm that non-solvated lead cations are indeed not intercalated in its structure.

The presence of LiF salt is evidenced even after several washing steps, before and after Pb uptake, by the sharp peaks at $2\theta=38^{\circ}$, 45° , and 66° . Small amounts of partially etched MAX phase can be identified by the sharp (002) peak at 9.5° , the small (101) peak at 34.5° , and the (110) peak at 61° . Other smaller peaks detected in both pristine and Pb-loaded material can be related to aluminum oxide (Al₂O₃) etching by-products. Finally, the additional peaks exclusively present in $Ti_3C_2T_x/Pb_{ads}$ were attributed to the uptake of lead iodide hydroxide, PbI(OH), which can be an indication of the formation of inner-sphere complexes mechanism upon lead capturing by MXenes. In this case, the different lead-iodine complexes present in the acetone could directly interact with functional groups

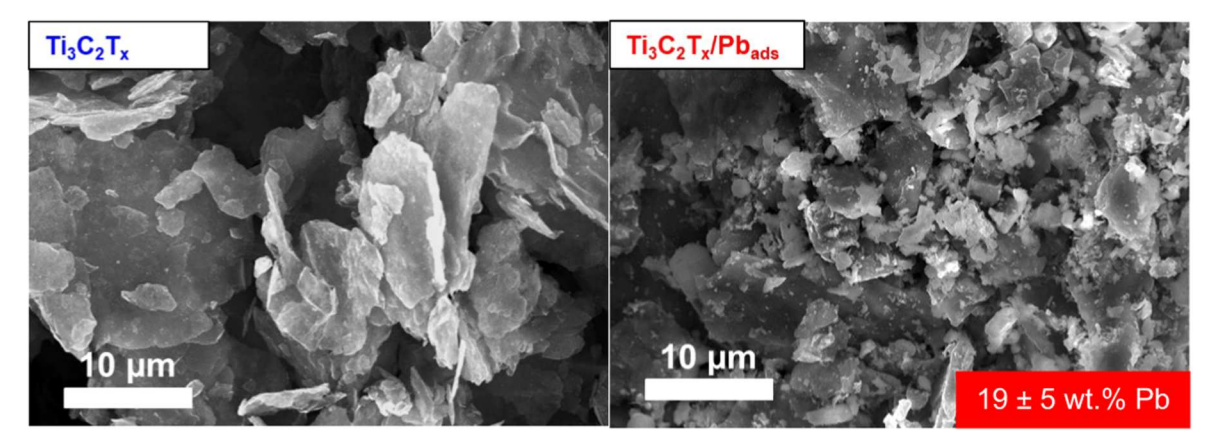


Figure 4. SEM micrographs of pristine Ti₃C₂T_x (blue) and Ti₃C₂T_x/Pb_{ads} (red).

on the MXene surface, forming a stable, covalent-like bond, which enhances lead adsorption capacity even with lower contact times. 52,59

No new peaks or bands were found by Fourier-transform infrared (FTIR) spectroscopy when comparing both materials, which is expected due to the nature of adsorption. Some of the vibrations related to -OH and -C-O functional groups at around $3300~\rm cm^{-1}$ and $1100~\rm cm^{-1}$, respectively, show a decrease in intensity for $Ti_3C_2T_x/Pb_{ads}$, which could indicate an interaction with adsorbed species (Fig. S1). The composition of both materials was obtained by energy-dispersive X-ray spectroscopy (EDX) and is shown in Table S1.

Overall, the adsorption of ca. 19 wt% of lead was confirmed by EDX analysis, representing one Pb atom for every five Ti atoms. The expected ratio of 1.5 for Ti/C atoms was close for $Ti_3C_2T_x/Pb_{ads}$ (Ti/C = 1.7), while for pristine $Ti_3C_2T_x$ (Ti/C = 2.2), it could imply the presence of some titanium oxide contamination. The presence of unetched MAX phase can be confirmed by the presence of small amounts of aluminum in both materials, and LiF is present in a significant amount since fluorine was found up to 35 wt% in $Ti_3C_2T_x/Pb_{ads}$. A small amount of iodine was also adsorbed from the Pb/acetone solutions, but the ratio of Pb/I atoms does not indicate the adsorption of PbI₂ salt.

No change in the morphology of MXene flakes was observed by scanning electron microscopy (SEM), but the presence of particle agglomerates deposited at the surface of the MXene plates can be seen (Fig. 4).

The particulate material was found to be fluorine-rich (Fig. S2 and Table S2), which could be an indication of the partial deintercalation of LiF from the MXene layers, coming to the surface of the material and not being washed away by the acetone, which is also supported by the high variability in fluorine content. Furthermore, some of the crystals seen in Fig. 4 can be attributed to PbI₂ and precipitated sodium salts that were also present in the Pb/acetone solution. Overall, the layered MXene structure was maintained even with the presence of lead and the other salts found after adsorption.

Electrochemical energy storage.—The recovered adsorbent loaded with lead was directly transformed into an active material for a supercapacitor electrode, *i.e.*, no further chemical processing, heat treatment, or energy input of any kind was necessary to convert the spent adsorbent into a functional electrode. The results of the electrochemical experiments are shown in Fig. 5.

While MXenes are known for their mainly pseudocapacitive behavior, 60 the cyclic voltammetry (CV) of ${\rm Ti}_3{\rm C}_2{\rm T}_x$ shows an almost rectangular profile, similar to that of electric double-layer capacitors (EDLCs) (Fig. 5a), without any distinct redox peaks. This is due to their fast redox reactions involving surface terminations taking place at the surface, coupled with their hydrophilic nature and the abundance of functional groups (–OH, –O, and –F). This provides

a capacitance of $70\,\mathrm{F\cdot g}^{-1}$ at $1\,\mathrm{mV\cdot s}^{-1}$, which is in agreement with the material's literature. A similar behavior is seen with increasing scan rate, where the average capacitance slightly decreases to $65\,\mathrm{F\cdot g}^{-1}$ at $10\,\mathrm{mV\cdot s}^{-1}$, but the rectangular shape is maintained (Fig. 5b).

 $Ti_3C_2T_x/Pb_{ads}$, however, provides not only the EDLC and pseudocapacitive response coming from the MXene matrix, but an additional pair of redox peaks appears starting from the first cycle (Fig. 5a). The charge contribution from the redox pair at -0.33 V vs SHE is assumed to come from:

$$Pb^{+2} + 2e^{-} \rightleftharpoons Pb^{0}$$
 [R1]

as the adsorbed lead cations are thus reduced to metallic lead and then oxidized back to the divalent form. From the first cycle, it is possible that the initial reduction starts below -0.43 V vs SHE, which is the thermodynamic value at this pH (Fig. S3). ⁶² The subsequent cycles present the redox pair at higher potentials, indicating the formation of some lead species more prone to oxidation.

Interestingly, the redox pair is visible even at 10 times the scan rate, pointing to fast reaction kinetics (Fig. 5b). The presence of lead does not decrease the MXene pseudocapacitive contribution, as the normalization by the mass of MXene in the active material proves on the extended-range CV shown in Fig. S4a. Furthermore, normalizing the capacity by the mass of MXene allows to verify that adsorbed lead is able to initially increase the capacity of the electrodes from $30~{\rm C} \cdot {\rm g}^{-1}$ up to $70~{\rm C} \cdot {\rm g}^{-1}$ from the second cycle, dropping after each cycle until a similar capacity to the pristine ${\rm Ti}_3 {\rm C}_2 {\rm T}_x$ is achieved after 10 cycles (Fig. S4b).

The initial capacity obtained for pristine Ti₃C₂T_x in the galvanostatic charge-discharge (GCPL) cycling at 50 mA·g⁻¹ was $27 \text{ C} \cdot \text{g}^{-1}$ within the studied potential window (Fig. 5c). The presence of lead, however, increased the initial capacity up to 60 C·g⁻¹ of total active material, meaning that even taking into account the mass of the heavy metal present in the recycled adsorbent, the charge storage capacity initially more than doubled. Clear plateaus can be seen in the Ti₃C₂T_x/Pb_{ads} GCPL curves, indicating a continuous and stable redox activity of this metal at well-defined potentials. When cycled faster at 100 mA·g⁻¹, both materials show a slight decrease in capacity, which is well recovered when cycling again at 50 mA·g⁻¹, but at a point where the faradaic contribution of Pb is no longer present due to cation dissolution in the electrolyte (Fig. 5d). It is necessary to mention that, besides cycling stability being a significant issue towards the practical feasibility of this system, rather than optimizing the electrochemical performance metrics at this early stage, we illustrate the feasibility of the concept, with the expectation that it will stimulate further work to improve performance.

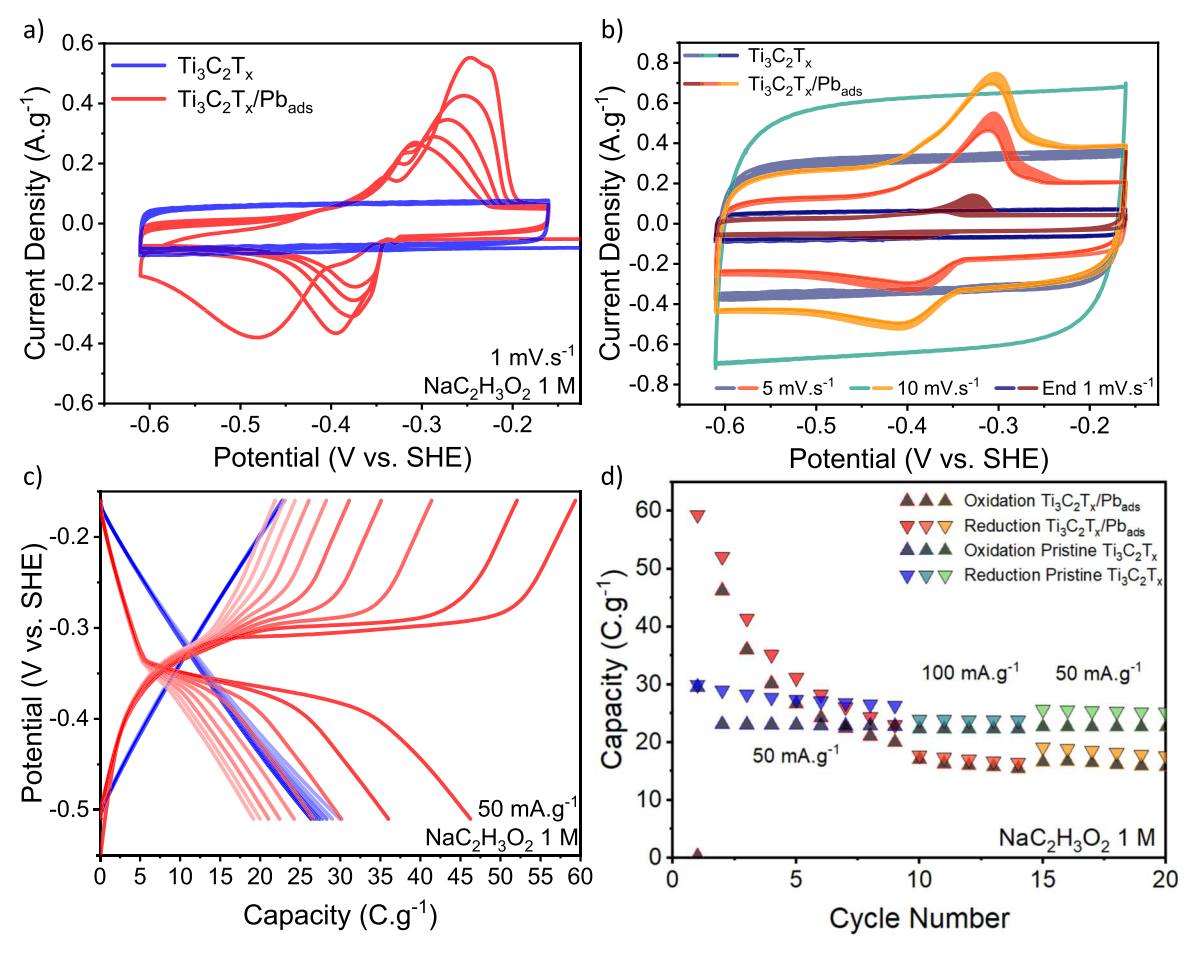


Figure 5. Upper: Cyclic voltammetry of the as-assembled $Ti_3C_2T_x$ electrode (blue) and $Ti_3C_2T_x/Pb_{ads}$ (red) in 1 M sodium acetate solution showing a) the first 5 cycles at 1 mV·s⁻¹, b) the 3rd cycles at 5, 10, and repeated at 1 mV·s⁻¹. lower: GCPL experiments of the pristine (blue) and Pb-loaded (red) MXene with c) the capacity retrieved on each cycle, excluding the first one at 50 mA·g⁻¹ of active material, and d) the calculated capacity from each cycle at 50 mA·g⁻¹, 100 mA·g⁻¹ and repeated at 50 mA·g⁻¹.

Conclusions

This study demonstrates a comprehensive approach for addressing two critical environmental and technological challenges: the sustainable recycling of perovskite solar cells and the development of new electrode materials for energy storage. In this study, acetone-based solvent was used on PbI solution to simulate lead capture from perovskite solar cell composition. By using MXenes - specifically $Ti_3C_2T_x$ synthesized via a LiF route -as efficient lead adsorbents from acetone-based solvent waste, we achieved exceptional lead removal efficiency (>99.9%), transforming a hazardous by-product into a value-added material ($Ti_3C_2T_x/Pb_{ads}$).

Achieving such a high lead removal from a high-concentration (100 ppm) acetone solution is an important result from a recycling perspective, since it allows for decreasing the toxicity level of the contaminated solutions produced by the recycling processes, consequently reducing the costs and complexity of disposing of them. ³⁵ Furthermore, a regenerated acetone solution with low residual lead content might be recovered and reused in the recycling process to dissolve additional PSC devices before their final disposal, thus reducing the overall solvent consumption and the environmental footprint of the process.

By valorizing the spent MXene material - now enriched with electrochemically active lead cations - employed directly as electrode material for supercapacitors, $Ti_3C_2T_x/Pb_{ads}$ exhibited significantly enhanced charge storage behavior, doubling the initial capacity compared to pristine $Ti_3C_2T_x$ by adding a reversible redox activity attributable to the adsorbed lead species to the capacitive and pseudocapacitive behavior of the MXene electrode. This

transformation from an environmental adsorbent to an energy storage component, besides requiring further validation using real PSC waste, highlights a powerful paradigm: converting waste into functionality and pollution into potential with minimal additional energy input. The integration of waste recovery and energy storage within a single process underscores the power of circular material strategies. This proof-of-concept not only presents a new method for recovering contaminated solvents but also reassures the reuse of these heavy-metal-laden adsorbents into new functional materials.

Experimental

Adsorption experiments.—The Pb/acetone solutions were made by dissolving carefully weighed amounts of high-purity lead iodide (Sigma Aldrich, PbI₂ 99.999% trace metals) into defined volumes of reagent-grade acetone (Sigma Aldrich, ACS reagent, ≥99.5%). Sodium iodide (Sigma Aldrich, NaI ReagentPlus®, ≥99%) was added to the solutions in a 1:2 weight ratio with lead iodide to overcome acetone's low solubility limit and to achieve the complete dissolution of the dissolved lead iodide thanks to the formation of iodoplumbate complexes. The solutions were then left stirring at room temperature—no heating was ever provided to accelerate the process—for at least 24 h to ensure a homogeneous chemical equilibrium in the dissociation reactions is achieved throughout the whole volume. The effective lead concentration of each solution was measured in triplicate by ICP-MS. A detailed summary of the parameters of the Pb/acetone solutions is presented in Table S3.

The samples for the absorption experiments were prepared in polypropylene vials (no potential lead leakage, unlike glass containers) by mixing appropriate amounts of MXene adsorbent powder into defined volumes of Pb/acetone solution to obtain the intended adsorbent doses. The vials—kept always closed to avoid any solvent evaporation and volume loss—were left stirring overnight at a controlled room temperature of 22 °C to ensure the adsorption process reached a homogeneous equilibrium throughout the whole volume. Control experiments were carried out alongside the adsorption ones, consisting of vials of Pb/acetone solution without the addition of any adsorbent powder. After equilibrium was reached, the supernatant was collected, and the solutions were diluted for the lead concentration measurements, as detailed below. When the used adsorbent was $Ti_3C_2T_x$ -LiF, the suspension was filtered through PVdF membranes, the residue was washed with clean acetone, and left to dry overnight in a vacuum oven at 80 °C to obtain the $Ti_3C_2T_x$ /Pb_{ads} powder.

The lead concentration measurements were performed using an Agilent 7800 ICP-MS instrument, equipped with an autosampler that facilitates processing a large number of samples and improves measurement reliability and repeatability. The instrument can precisely measure elemental concentrations below the parts per billion (ppb) range with high precision, but can only process low concentration solutions (below 100 ppb) of aqueous media, preferably based on diluted nitric acid. Since the Pb/acetone solutions have lead concentration values in the range of 50 to 300 parts per million (ppm), a common dilution ratio of 1:40000 was chosen, achieved by two 1:200 dilution steps in cascade. The first dilution step was performed by adding 50 µL of the study solution into a vial with 9.95 mL of 2.5% nitric acid solution, obtaining a 10 mL solution with a 1:200 dilution ratio; for the second step, 50 µL of the previous solution were added to a vial containing 9.85 mL of 2.5% nitric acid solution and 100 µL of yttrium standard solution (Sigma Aldritch, TraceCERT®, 1000 mg·L⁻¹ Y in nitric acid) diluted at 100 ppb, used as the internal standard for the ICP-MS measurements to provide an additional degree of reliability and robustness. With these two steps, the final dilution ratio of 1:40000 is achieved. To ensure no additional contaminants are introduced by the dilution process, the nitric acid solution employed is made with spectroscopic grade nitric acid (Fluka, TraceSELECT™ for trace analysis, ≥69.0%) and ultrapure distilled water. The ICP-MS setup is calibrated using a six-point calibration curve: a lead standard solution for ICP-MS (Sigma Aldritch, TraceCERT®, 1000 mg·L⁻¹ Pb in nitric acid) is diluted from its initial concentration of 1000 ppm to adequate values (0, 0.1, 0.5, 1, 5, 10 ppb), using the same diluted nitric acid and yttrium internal standard. The actual lead concentration values of the Pb/acetone solutions are then calculated by multiplying the values measured via ICP-MS by the dilution factor of 40000, taking into account the error propagation.

Synthesis procedures.—Synthesis of reduced graphene oxide (rGO).—The preparation of rGO was carried out following a previously reported method.³² Briefly, graphene oxide (GO) was produced from graphite powder using a modified Hummers method and maintained as an aqueous suspension at a concentration of 1 mg·mL⁻¹. For the reduction process, 35 mL of the GO suspension was transferred into 50 mL Teflon-lined autoclaves and subjected to hydrothermal treatment at 180 °C for 12 h. The resulting rGO foam was thoroughly washed with deionized water and then freeze-dried.

Synthesis of MXenes.— 31,46 Both $Ti_3C_2T_x$ MXenes synthesis routes started by treating titanium aluminum carbide 312 (Ti_3AlC_2 MAX phase, Sigma Aldrich $\geqslant 90\%$) with 9 M hydrochloric acid (HCl, $\sim 37\%$, Fisher Chemical) at room temperature overnight (around 18 h) using 25 mL of acid for every 1 g of MAX. This pre-etching step is important for removing non-stoichiometric phases, such as $TiAl_3$ and intermetallic impurities, from the starting product. The powder was then thoroughly washed with DI water (around 250 mL per 1 g of MAX) until a neutral pH was reached, and then filtered and dried at 60 °C for further etching processes. The other reagents were used without further purification.

 $Ti_3C_2T_x$ - NH_4HF_2 .—The synthesis was conducted via wet chemical etching of Ti₃AlC₂ MAX phase powder with a particle size of ≤200 µm. The etching solution precursor was prepared by separately dissolving 7.3 g of ammonium bifluoride (NH₄HF₂, 95% Alfa Aesar) in 100 mL of DI water and 5 g of citric acid (C₆H₈O₇, 99.5% anhydrous, Thermo Scientific) in 200 mL of DI water. The two solutions were carefully mixed in an HDPE container under constant stirring at room temperature, to which 4 g of the pre-washed dried MAX phase powder was slowly added. The reaction mixture was stirred for 72 h, with the lid loosely covered to allow gas escape generated during etching. The resultant suspension was washed with DI water through several cycles of centrifugation at 5,000 rpm for 5 min until the supernatant was at pH \sim 5, when the upper part of the slurry was collected for delamination. The wet powder was added to a 300 mL solution with 4 mL of tetramethylammonium hydroxide (TMAOH, 25% in water, Sigma-Aldrich) and was left stirring for 72 h at room temperature. After that time, the suspension was sonicated for 3 h for further delamination and centrifuged at 10,000 rpm for 15 min for 3 washing cycles. At each cycle, the volume was replaced with DI water to remove the intercalated TMAOH. Finally, the delaminated material was collected on 3 collection centrifugation cycles at 3,000 rpm for 5 min, where the supernatant was kept and the decanted slurry washed again. The collected supernatant suspension was then filtered through PVdF membranes (0.45 µm, hydrophilic, Durapore) and washed again with distilled water. The nanosheets were dried under vacuum at 80 °C for 24 h to remove residual water, resulting in carboxylic-terminated Ti₃C₂T_x-NH₄HF₂ powder.

 $Ti_3C_2T_x$ -LiF.—The etching solution was first prepared by dissolving 4.8 g of lithium fluoride (LiF, >99%, Honeywell Fluka) in 60 mL of 9 M HCl under continuous stirring for 5 min. Subsequently, 3 g of pre-washed MAX phase powder with a particle size of $\leq 40 \,\mu \text{m}$ was gradually added to the etchant. The resulting mixture was left stirring at room temperature for 24 h. The acidic suspension was washed 3 times with deionized water through repeated centrifugation steps at 5,000 rpm for 5 min. After each cycle, the supernatant was decanted and replaced with fresh deionized water before the next cycle. Washing was continued until the pH of the suspension reached around 5, when the sediment at the bottom of the centrifuge tube started swelling into a black slurry layer of delaminated Ti₃C₂T_x above a greyish layer of residual Ti₃AlC₂/Ti₃C₂T_x material. The top black Ti₃C₂T_x slurry was collected with a spatula, resuspended in DI water, and subjected again to centrifugation at 2500 rpm for 5 min, followed by vacuum filtration of the supernatant suspension. The filtered material was dried under vacuum at 80 °C for 24 h, resulting in the formation of Ti₃C₂T_x-LiF powder.

Materials characterization.—Scanning electron microscopy & energy dispersive X-ray spectroscopy (SEM/EDX).—SEM images were obtained with a Zeiss Merlin instrument at 20 kV, and EDX analysis was conducted with an OXFORD Instruments device, 50 mm² X-Max detector at 8 mm working distance.

X-ray diffraction (XRD).—X-ray diffraction patterns were obtained using a PANalytical X'Pert Pro-diffractometer (Malvern Panalytical, Almelo, Netherlands) with a radiation source of Cu–K α 1–K α 2 (λ = 1.54060, 1.54443 Å) and a voltage of 40 kV at a current of 40 mA. Data were recorded on powder samples using a 2 theta range of 5–80°.

Raman spectroscopy.—Raman spectra were taken in 15 accumulations of 30 s from 50 to 2350 cm⁻¹ using a Horiba LabRAM HR Evolution Raman microscope spectrometer. The device was equipped with a Syncerity OE detector with an ADC rate of 45 kHz and a 633 nm He-Ne red laser source. The laser power at the sample was attenuated using a 3.2% neutral density (ND) filter, and spectra were acquired using a 300 grooves mm⁻¹ grating

optimized for the visible range, and a 50× long working distance VIS objective.

Fourier-transform infrared (FTIR) spectroscopy.—A Bruker IFS 66v/S spectrometer equipped with a single-reflection diamond crystal attenuated total reflectance (ATR) accessory (GoldenGate, Specac) was used to carry out measurements in the range of 4000–400 cm⁻¹ accumulated for 64 scans. The spectrometer utilized an aperture of 8 mm, a Globar source with a DTGS detector, and a potassium bromide (KBr) beamsplitter.

Electrochemistry.— *Electrode preparation.*—Ti₃C₂T_x and Ti₃C₂T_x/ Pb_{ads} electrodes were prepared respectively from the Ti₃C₂T_x-LiF powder before adsorption or from the recovered powder containing lead (Ti₃C₂T_x/Pb_{ads}). The active material was mixed with carbon black (PUREBLACK 205-110 Carbon, Superior Graphite Co., IL, USA) and PTFE binder (60% w/w aq. sol., Sigma Aldrich) at a 7:2:1 mass ratio. The resulting slurry was dispersed in ethanol, stirred until dry, and coldrolled into self-standing films (\sim 100 μ m thick) using a glass bar. Diskshaped electrodes (10 mm diameter) of around 2 mg were punched from these films.

Activated carbon (AC) was used to prepare thick counter electrodes by mixing AC YP50 (Kuraray Chemicals), carbon black, and PTFE binder at an 85:10:5 mass ratio in ethanol, then drying the mixture. The electrodes were shaped to be over 1 mm thick, ensuring a mass at least 15 times that of the working electrodes. Finally, 12 mm diameter self-standing AC electrodes were cut.

Cell assembly.—A 3-electrode setup in Swagelok-type cells was used for electrochemical characterization. Two glass microfiber separators (GF-D 1172-4113, Fisherbrand) were placed between the self-standing working electrode and an AC thick counter electrode, with excess electrolyte. A reference electrode (Hg/Hg₂SO₄ in sat. K₂SO₄) was placed in the cell upper aperture.

Measurements.—Cyclic voltammetry (CV) and galvanostatic charge/discharge with potential limitation (GCPL) were performed using a VMP3 potentiostat (Biologic, operated under ECLab software version V11.50) in an air-conditioned room (22 °C).

Acknowledgments

As a part of the DESTINY PhD program, this publication is acknowledged by funding from the European Union's Horizon 2020 research and innovation program under the Marie Skłodowska-Curie Actions COFUND (Grant Agreement #945357). Conseil Régional des Pays de la Loire is also acknowledged for supporting this PhD project. The authors are also grateful for the financial support from the Swedish Research Council (VR) Distinguished Professor grant "Next Generation Batteries" (#2021-00613). The authors would like to acknowledge the support of colleagues such as Camille Douard, Gabriella Schirinzi, and Guillaume Baucher for all the cooperative work done.

CRediT Author Contributions

Marcelo A Andrade: Investigation, Methodology, Formal Analysis, Visualization, Writing-original draft; Alessandro Mezzetti: Investigation, Methodology, Writing-original draft; Francesco Fumagalli: Review & editing, Supervision; Giacomo Ceccone: Conceptualization; Olivier Crosnier: Conceptualization, Review & editing, Supervision; Patrik Johansson: Validation, Review & editing; Thierry Brousse: Conceptualization, Project administration, Review & editing, Supervision;

ORCID

Marcelo A. Andrade https://orcid.org/0009-0003-7811-872X Alessandro Mezzetti https://orcid.org/0000-0001-5653-4317 Francesco Fumagalli https://orcid.org/0000-0003-2172-9469

Giacomo Ceccone https://orcid.org/0000-0003-4637-0771 Olivier Crosnier https://orcid.org/0000-0001-6747-9413 Patrik Johansson https://orcid.org/0000-0002-9907-117X Thierry Brousse https://orcid.org/0000-0002-1715-0377

References

- 1. A. Kojima, K. Teshima, Y. Shirai, and T. Miyasaka, "Organometal halide perovskites as visible-light sensitizers for photovoltaic cells." J. Am. Chem. Soc., 131. 6050 (2009).
- 2. C. Yang et al., "Achievements, challenges, and future prospects for industrialization of perovskite solar cells." Light: Sci. Appl., 13, 227 (2024).
- 3. K. A. Parrey et al., "Synthesis and characterization of an efficient hole-conductor free halide perovskite CH3NH3PbI3 semiconductor absorber based photovoltaic device for IOT synthesis and characterization of an efficient hole-conductor free halide perovskite CH₃NH₃Pb." Journal of The Electrochemical Society, **165**, B3023 (2018).
- 4. J. Liu, M. Lei, and G. Wang, "Communication-Enhancing hole extraction in carbon-based CsPbBr3 inorganic perovskite solar cells without hole-transport
- layer," ECS J. Solid State Sci. Technol., 9, 041004 (2020).

 5. G. A. AlZaidy and H. T. A. Alanazi, "Review—Recent advancements in perovskites solar cell materials and the investigation of transition metal oxide-based nanocomposites for usage in perovskites solar cells." ECS J. Solid State Sci. Technol., 13, 055006 (2024).
- S. Yanagida, S. Yanagisawa, M. Yanagida, and H. Segawa, "Computational verification of so-called perovskite solar cells as PbI₆⁴⁻-Aligned solar cells." ^t. Electrochem. Soc., **164**, E3598 (2017).
- 7. R. I. Maphoto, M. T. Morukuladi, K. T. Malatji, M. C. Masedi, and P. E. Ngoepe, "First-principle study of CsPbBr₃ and CsPbI₃ perovskite solar cells." ECS J. Solid State Sci. Technol., 11, 035012 (2022).
- 8. F. Bouhjar, M. Mollar, S. Ullah, B. Marí, and B. Bessaïs, "Influence of a compact α-Fe₂O₃ layer on the photovoltaic performance of perovskite-based solar cells." Electrochem. Soc., 165, H30 (2018).
- 9. H. Jian et al., "Conjugated polyelectrolyte combined with ionic liquid as the hole transport layer for efficient inverted perovskite solar cells." J. Electrochem. Soc., **168**, 036503 (2021).
- Z. Wang et al., "Lead-tin laminated all-perovskite solar cells: verification of feasibility from the perspective of device simulation." ECS J. Solid State Sci. Technol., 11, 063011 (2022).
- 11. R. G. Charles, A. Doolin, R. García-Rodríguez, K. V. Villalobos, and M. L. Davies, "Circular economy for perovskite solar cells - drivers, progress and challenges." Energy Environ. Sci., 16, 3711 (2023).
- 12. A. Babayigit et al., "Assessing the toxicity of Pb-and Sn-based perovskite solar cells in model organism danio rerio." Sci. Rep., 6, 1 (2016).
- 13. L. Huang et al., "New films on old substrates: Toward green and sustainable energy production via recycling of functional components from degraded perovskite solar cells." ACS Sustain. Chem. Eng., 5, 3261 (2017).
- 14. D. S. Lee et al., "Green solvent strategies for the sustainable development of perovskite solar cells." Chem. Commun., 61, 2011 (2025).
- S. Y. Park et al., "Sustainable lead management in halide perovskite solar cells." Nat. Sustain., 3, 1044 (2020).
- 16. J. Walzberg, A. Carpenter, and G. A. Heath, "Role of the social factors in success of solar photovoltaic reuse and recycle programmes." Nat. Energy, 6, 913 (2021).
- 17. Q. Li et al., "MXenes-based adsorbents for environmental remediation." Sep. Purif. Technol., 342, 126982 (2024).
- 18. M. A. Andrade, O. Crosnier, P. Johansson, and T. Brousse, "Designing an electrochemical energy storage device using recycled $\text{Ti}_3\text{C}_2\text{T}_x$ MXene and reduced graphene oxide spent wastewater adsorbents." Electrochim. Acta, 540, 147176 (2025).
- 19. J. Come et al., "A non-aqueous asymmetric cell with a Ti₂C-based two-dimensional negative electrode." J. Electrochem. Soc., 159, A1368 (2012).
- 20. K. Kim, M. Okubo, and A. Yamada, "Interfacial dissociation of contact-ion-pair on mxene electrodes in concentrated aqueous electrolytes." J. Electrochem. Soc., 166,
- 21. S. A. Melchior et al., "High-voltage symmetric supercapacitor based on 2D titanium carbide (MXene, Ti₂CT_x)/carbon nanosphere composites in a neutral aqueous electrolyte." J. Electrochem. Soc., 165, A501 (2018).
- 22. M. Cao et al., "Room temperature oxidation of Ti₃C₂ MXene for supercapacitor electrodes." J. Electrochem. Soc., 164, A3933 (2017).
- 23. Y. Zhu et al., "MnO₂ -MXene composite as electrode for supercapacitor." Electrochem. Soc., 169, 030524 (2022).
- 24. Y. Fang et al., "MXene-derived TiO2/reduced graphene oxide composite with an enhanced capacitive capacity for Li-ion and K-ion batteries." J. Mater. Chem. A, 7, 5363 (2019).
- 25. Q. Peng et al., "Unique lead adsorption behavior of activated hydroxyl group in two-
- dimensional titanium carbide." *J. Am. Chem. Soc.*, **136**, 4113 (2014).

 26. M. A. Andrade, A. L. Bugaev, A. Skorynina, and C. Douard, "Tracking Hg²⁺ adsorption by reduced graphene oxide in continuous flow by in situ techniques." J. Environ. Chem. Eng., 13, 118680 (2025).
- 27. L. Wang, M. Han, C. E. Shuck, X. Wang, and Y. Gogotsi, "Adjustable electrochemical properties of solid-solution MXenes." Nano Energy, 88, 106308
- 28. P. Simon and Y. Gogotsi, "Perspectives for electrochemical capacitors and related devices." Nat. Mater., 19, 1151 (2020).

- B. Anasori, M. R. Lukatskaya, and Y. Gogotsi, "2D metal carbides and nitrides (MXenes) for energy storage." Nat. Rev. Mater., 2, 16098 (2017).
- M. A. Andrade et al., "Synthesis of 2D solid-solution (Nb_yV_{2-y})CT_x MXenes and their transformation into oxides for energy storage." ACS Appl. Nano Mater., 6, 16168 (2023).
- S. Shah, I. Mubeen, E. Pervaiz, and H. Nasir, "Enhanced removal of toxic Cr(vi) and Pb(ii) from water using carboxylic terminated Ti₃C₂T_x nanosheets." *RSC Adv.*, 13, 23320 (2023).
- M. A. Andrade, O. Crosnier, P. Johansson, and T. Brousse, "Energy from garbage: recycling heavy metal-containing wastewater adsorbents for energy storage." Adv. Energy Sustain. Res., 2400195, 6 (2024).
- A. Mezzetti et al., "Acetone as an inexpensive, green solvent for perovskite solar cell recycling." *International Conference on Hybrid and Organic Photovoltaics* (HOPV24), València, SpainMay 12th - 15th (2024), in Presentation 091.
- V. Larini et al., "Sustainable and circular management of perovskite solar cells via green recycling of electron transport layer-coated transparent conductive oxide." *Adv. Funct. Mater.*, 34, 2306040 (2024).
- Agency, C. & Directives, C. Commission Regulation (EU), "2015/628 of 22 April 2015 amending Annex XVII to regulation (EC) No 1907/2006 of the European parliament and of the council on the registration, evaluation, authorisation and restriction of chemicals ("REACH") as regards lead an." Off. J. Eur. Union L, 104, 2 (2015).
- X. Xu et al., "A power pack based on organometallic perovskite solar cell and supercapacitor." ACS Nano. 9, 1782 (2015).
- Z. Liu et al., "Novel integration of perovskite solar cell and supercapacitor based on carbon electrode for hybridizing energy conversion and storage." ACS Appl. Mater. Interfaces, 9, 22361 (2017).
- S.-J. Park et al., "Review—A review of advanced electronic applications based on carbon nanomaterials." ECS J. Solid State Sci. Technol., 9, 071002 (2020).
- Z. Song et al., "Photocapacitor integrating perovskite solar cell and symmetrical supercapacitor generating a conversion storage efficiency over 20%." Nano Energy, 100, 107501 (2022).
- W. R. Gallegos-Pérez et al., "A simplified equivalent circuit model for the photocharging process of carbon-based quasi-solid photosupercapacitors." ECS J. Solid State Sci. Technol., 12, 115003 (2023).
- Y. Yang et al., "Efficient self-charging monolithic photocapacitors comprised of perovskite solar cell and quasi-solid-state supercapacitor through a shared Janus carbon electrode." Chem. Eng. J., 510, 161737 (2025).
- S. A. Fateev, E. I. Marchenko, A. A. Petrov, E. A. Goodilin, and A. B. Tarasov, "New acidic precursor and acetone-based solvent for fast perovskite processing via proton-exchange reaction with methylamine." *Molecules*, 25, 1 (2020).
- R. K. Jena, H. T. Das, B. N. Patra, and N. Das, "MXene-based nanomaterials as adsorbents for wastewater treatment: A review on recent trends." *Front. Mater. Sci.*, 16, 1 (2022).
- C. Gao, Z. Dong, X. Hao, Y. Yao, and S. Guo, "Preparation of reduced graphene oxide aerogel and its adsorption for Pb(II)." ACS Omega, 5, 9903 (2020).

- K. Matthews, T. Zhang, C. E. Shuck, A. Vahidmohammadi, and Y. Gogotsi, "Guidelines for synthesis and processing of chemically stable two-dimensional V2CTxMXene." *Chem. Mater.*, 34, 499 (2022).
- M. Downes, C. E. Shuck, B. McBride, J. Busa, and Y. Gogotsi, "Comprehensive synthesis of Ti₃C₂T_x from MAX phase to MXene." *Nat. Protoc.*, 19, 1807 (2024).
- A. Sarycheva and Y. Gogotsi, "Raman spectroscopy analysis of the structure and surface chemistry of Ti₃C₂T_x MXene." *Chem. Mater.*, 32, 3480 (2020).
- T. Parker et al., "In situ raman and fourier transform infrared spectroscopy studies of MXene—electrolyte interfaces." ACS Nano, 19, 22228 (2025).
- S. Adomaviciute-Grabusove et al., "Monitoring Ti₃C₂T_x MXene degradation pathways using raman spectroscopy." ACS Nano, 18, 13184 (2024).
- E. H. Driscoll, A. Orera, P. A. Anderson, M. L. Sanjuán, and P. R. Slater, "Raman spectroscopy insights into the α- and δ-phases of formamidinium lead iodide (FAPbI₃)." *Dalt. Trans.*, 50, 3315 (2021).
- A. Kagalkar, S. Dharaskar, N. Chaudhari, V. Vakharia, and R. R. Karri, "Enhanced metal ion adsorption using ZnO-MXene nanocomposites with machine learningbased performance prediction." Sci. Rep., 15, 15563 (2025).
- A. Kagalkar, S. Dharaskar, and N. Chaudhari, "Development of MXene for removal of lead (Pb⁺) ions from wastewater." Water Pract. Technol., 19, 911 (2024).
- M. Shekhirev, C. E. Shuck, A. Sarycheva, and Y. Gogotsi, "Characterization of MXenes at every step, from their precursors to single flakes and assembled films." *Prog. Mater Sci.*, 120, 100757 (2021).
- R. Rakhmanov et al., "Influence of MXene interlayer spacing on the interaction with microwave radiation." Adv. Funct. Mater., 2410591, 1 (2024).
- Q. Gong et al., "Thorium-doped lithium fluoride single crystal: a potential promising candidate for solid state nuclear optical clock materials." Adv. Opt. Mater., 11, 1 (2023).
- M. Anayee, M. Shekhirev, R. Wang, and Y. Gogotsi, "Effect of oxygen substitution and oxycarbide formation on oxidation of Ti₃AlC₂ MAX phase." *J. Am. Ceram.* Soc., 107, 6334 (2024).
- N. Mozaffari, A. Haji Seyed Mirzahosseini, A. H. Sari, and L. Fekri Aval, "Investigation of carbon monoxide gas adsorption on the Al₂O₃/Pd(NO₃)₂/zeolite composite film." *J. Theor. Appl. Phys.*, 14, 65 (2020).
- M. Salavati-Niasari and F. Tavakoli, "Pb(OH)l-graphene composite: synthesis and characterization." J. Ind. Eng. Chem., 21, 1208 (2015).
- B.-M. Jun, N. Her, C. M. Park, and Y. Yoon, "Effective removal of Pb(II) from synthetic wastewater using Ti₃C₂T_x MXene." *Environ. Sci. Water Res. Technol.*, 6, 173 (2020).
- C. Zhan et al., "Understanding the MXene pseudocapacitance." J. Phys. Chem. Lett., 9, 1223 (2018).
- Y. Zhu et al., "Modifications of MXene layers for supercapacitors." Nano Energy, 73 (2020).
- N. Takeno, Atlas of Eh-pH diagrams Geological Survey of Japan Open File Report No 419, National Institute of Advanced Industrial Science and Technology (May 2005), Intercomparison of thermodynamic databases.